ANNUAL REVIEWS

*Annual Review of Chemical and Biomolecular Engineering*

# Possibilities and Limits of Computational Fluid Dynamics–Discrete Element Method Simulations in Process Engineering: A Review of Recent Advancements and Future Trends

Paul Kieckhefen, Swantje Pietsch, Maksym Dosta, and Stefan Heinrich

Institute of Solids Process Engineering and Particle Technology, Hamburg University of Technology, 21073 Hamburg, Germany; email: paul.kieckhefen@tuhh.de

Annu. Rev. Chem. Biomol. Eng. 2020. 11:397–422

First published as a Review in Advance on March 13, 2020

The *Annual Review of Chemical and Biomolecular Engineering* is online at chembioeng.annualreviews.org

https://doi.org/10.1146/annurev-chembioeng-110519-075414



## Keywords

computational fluid dynamics, discrete element method, CFD-DEM, fluidization, granular dynamics, particulate flow

## Abstract

Fluid–solid systems play a major role in a wide variety of industries, from pharmaceutical and consumer goods to chemical plants and energy generation. Along with this variety of fields comes a diversity in apparatuses and applications, most prominently fluidized and spouted beds, granulators and mixers, pneumatic conveying, drying, agglomeration, coating, and combustion. The most promising approach for modeling the flow in these systems is the CFD-DEM method, coupling computational fluid dynamics (CFD) for the fluid phase and the discrete element method (DEM) for the particles. This article reviews the progress in modeling particle–fluid flows with the CFD-DEM method. A brief overview of the basic method as well as methodical extensions of it are given. Recent applications of this simulation approach to separation and classification units, fluidized beds for both particle formation and energy conversion, comminution units, filtration, and bioreactors are reviewed. Future trends are identified and discussed regarding their viability.

## 1. INTRODUCTION

The design and integration of solids processing equipment is a notable issue in the process industries. Merrow (1) identified solids processing steps as the primary determinant of delayed start-up times in newly constructed plants and below-specification performance over a chemical plant's lifetime. As such, the devotion of resources to the development and application of simulation methods such as computational fluid dynamics (CFD)-discrete element method (DEM) for the design of apparatuses is well justified.

Development of the CFD-DEM method started with Tsuji et al.'s (2, 3) pioneering work with 2D simulations, involving little physical modeling beyond pure dynamics due to limited computational resources. With the increasing availability in computational power, simulations of larger apparatuses and more comprehensive physical models have become commonplace. The CFD-DEM approach is now present in most major CFD packages, such as ANSYS Fluent, Siemens STAR-CCM+, and OpenFOAM, as well as in specialized ones like MFiX and CFDEMcoupling, and simulations can be set up in the time span of a few hours. As such, the barrier to entry has been lowered, and a wide range of studies and methodical extensions have blossomed in the field of particle–fluid interaction.

The central intention of this review is to provide a point of entry for applied researchers with little background in the field looking for an overview of the method's major applications. This contribution is divided into three sections: a brief overview of the method and general mathematical formulation, a broad review of recent applications as categorized by apparatus/functions, and our perspective on future trends.

## 2. METHOD OVERVIEW

### 2.1. Basics and Relation to Other Methods

The classical, unresolved CFD-DEM method, also referred to as the discrete-particle model, calculates the flow of a fluid using CFD methods in a continuum and the motion of particles as a discrete set of point masses. This section introduces the concept behind the method and its relation to other methods that follow similar principles, as well as its mathematical formulation.

**2.1.1. Concept.** The interaction between both phases is realized by mapping and interpolation procedures, excellently outlined by Radl et al. (4). In detail, the flow will merely experience the presence of the particles in the displacement of fluid in the pressure/continuity equation and the presence of momentum exchange terms. In turn, the particles will experience hydrodynamical forces and torques owing to fluid motions, the most prominent of which is drag force. Drag force is greatly dependent on the structure of the surrounding flow, which is usually collapsed to the solids volume fraction—often the same that is used in the momentum equations. The literature frequently differentiates between one-way, two-way, and four-way coupling that takes place between particles and fluids. One-way coupling refers to tracking particles through a flow field without considering the influence of the presence of the particles on the fluid phase. This is a reasonable assumption for situations with low solids volume fractions. With larger solids volume fractions, the influence of the particle phase becomes non-negligible, and two-way coupling with representation of the particles' influence on the flow field is required for accurate depiction of the system dynamics. There is a degree of uncertainty around the terminology: Some authors label such coupling schemes as four-way to denote particle–particle interactions, i.e., collisions. There is no consensus on the differentiation between two- and four-way coupling.

**2.1.2. Relation to other methods.** Along with the unresolved CFD-DEM method, microscale methods like the resolved CFD-DEM method and lattice Boltzmann–DEM method can be used

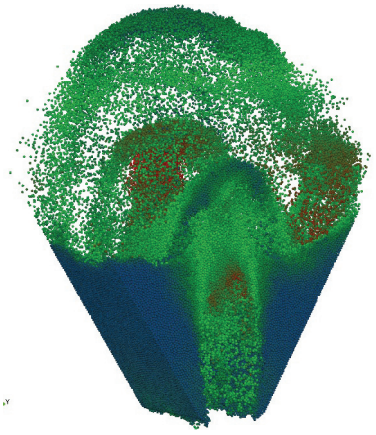

**Figure 1**

Snapshot of a computational fluid dynamics–discrete element method (CFD-DEM) simulation of a pseudo 2D-spouted bed. Reproduced with permission from Reference 11; copyright 2015 Elsevier.

to model particulate flows with resolved particle–fluid interaction. These methods do not require drag closures because particles are represented not by point masses but by considering their shape in the grid and imposing no-slip conditions at the boundary. This greatly increases accuracy, though at a computational cost that limits their applicability to very small apparatuses and short simulation time spans.

The multiphase particle-in-cell (MP-PIC) method and two-fluid model (TFM) target larger apparatuses and time spans. These methods model collisions instead of resolving them directly. The MP-PIC method (5, 6) solves equations of motion for particles that resemble those of CFD-DEM but do not include contact forces. Instead, a solids volume fraction–dependent interparticle stress is introduced that aims to prevent the overpacking of cells beyond the close-pack volume fraction. In the TFM (7), the solid phase is treated as a continuum that follows the laws of the kinetic theory of granular flow. This approach introduces a bulk solid viscosity and shear viscosity that depend on a set of closures that track the transport and dissipation of granular kinetic energy within a continuum. Modeling the consequence of collisions, rather than resolving them, gives both methods a clear advantage in terms of time scales that can be covered but requires diligence in the choice of appropriate closures for the flow regime at hand. For example, TFM is well equipped to model both nonfluidized, dense granular flow (8) and fluidized systems on their own with appropriate closures (9), but it finds its limit in the application to spouted beds (10), because this apparatus contains both flow regimes simultaneously. Regarding spouted beds, both Gryczka et al. (10) and Salikov et al. (11) treated the same system using TFM and CFD-DEM, respectively, with Salikov finding excellent agreement between simulations and experiment for the resulting visual system behavior (**Figure 1**), as well as the Fourier transform of the bed pressure drop that is a system characteristic.

**2.1.3. Mathematical formulations.** The soft-sphere DEM that is commonly used in CFD-DEM coupling can be summarized using the Newtonian equations of motion for any particle $i$ with mass $M_i$,

$$\ddot{\boldsymbol{x}}_i = \frac{1}{M_i}\left(\sum_{\text{particles/walls } j \text{ interacting with } i} \boldsymbol{F}_{j\to i} + \boldsymbol{F}_i^{\text{external}} + \boldsymbol{F}_i^{\text{fluid}}\right), \qquad 1.$$

**Table 1 List of symbols**

| Symbol | Definition | Unit |
|---|---|---|
| **Roman letters** | | |
| $C_f$ | Heat capacity of the fluid phase | Kg/m$^3$ |
| $d_p$ | Particle diameter | m |
| $e$ | Internal energy | J/m$^3$ |
| $\boldsymbol{F}_{drag}$ | Drag force | N |
| $\boldsymbol{F}^{external}$ | External force | N |
| $\boldsymbol{F}^{fluid}$ | Fluid interaction forces | N |
| $\boldsymbol{F}_{j\to i}$ | Particle–particle/particle–wall interaction forces | N |
| $\boldsymbol{g}$ | Gravitational acceleration | m²/s |
| $\boldsymbol{J}$ | Inertia tensor | kg·m²/rad |
| $M$ | Mass | kg |
| $p$ | Pressure | Pa |
| $\dot{Q}_{p\to f}$ | Heat flow from particle to fluid | W |
| Re | Reynolds number | - |
| $\dot{\boldsymbol{S}}$ | Momentum exchange term | kg·s/m³ |
| $\dot{S}_{particles,y_m}$ | Source term: fluid-phase material of species $m$ that is exchanged with the particle | kg/s |
| $\dot{S}_{reactions,y_m}$ | Source term: fluid-phase chemical conversion of species $m$ | kg/s |
| $t$ | Time | s |
| $\boldsymbol{T}^{fluid}$ | Torque induced by fluid | Nm |
| $\boldsymbol{T}_{j\to i}$ | Torque induced by particle–particle/particle–wall interaction | Nm |
| $\boldsymbol{u}$ | Velocity | m/s |
| $V_{cell}$ | Cell volume | m³ |
| $\ddot{\boldsymbol{x}}$ | Acceleration | m/s² |
| $y_m$ | Mass fraction of species $m$ | - |
| **Greek letters** | | |
| $\alpha_f$ | Fluid volume fraction | - |
| $\alpha_p$ | Particle volume fraction | - |
| $\beta$ | Momentum exchange coefficient | kg/m² |
| $\delta$ | Coarse-graining scaling factor | - |
| $\kappa$ | Thermal conductivity | W/(m·K) |
| $\mu_f$ | Dynamic viscosity of the fluid | kg/(m·s) |
| $\rho$ | Density | kg/m³ |
| $\boldsymbol{\tau}$ | Stress tensor | kg/s² |
| $\phi_{i,j}$ | Numerical weight | - |
| $\dot{\boldsymbol{\omega}}$ | Angular acceleration | rad/s² |

that include the three major components of the particle–particle and particle–wall interaction forces $\boldsymbol{F}_{j\to i}$, external forces $\boldsymbol{F}_i^{external}$, and fluid interaction forces $\boldsymbol{F}_i^{fluid}$ (**Table 1**). Similar equations are solved for rotational motion,

$$\dot{\boldsymbol{\omega}}_i = \frac{1}{J_i}\left(\sum_j \boldsymbol{T}_{j\to i} + \boldsymbol{T}_i^{fluid}\right), \qquad 2.$$

where $\boldsymbol{\omega}_i$ is the rotational motion, $\boldsymbol{T}_{j\to i}$ is torques induced by particle–particle and particle–wall interactions, and $\boldsymbol{T}_i^{\text{fluid}}$ is torque caused by fluid. Both equations are time integrated using symplectic integrators like leapfrog or the Verlet method. The interactions are modeled using contact laws that relate the overlap and relative velocities to the contact force $\boldsymbol{F}_{i\to j}$ in both normal and tangential direction of the contact. The most common contact models are the viscoelastic linear spring-dashpot and the nonlinear Hertz–Mindlin models.

Fluid flow in CFD-DEM coupling is usually resolved by applying the finite volume method to the Navier–Stokes equations to yield a velocity field $\boldsymbol{u}_\text{f}$:

$$\frac{\partial \alpha_\text{f} \rho \boldsymbol{u}_\text{f}}{\partial t} + \nabla \cdot \alpha_\text{f} \rho \boldsymbol{u}_\text{f} \boldsymbol{u}_\text{f} = -\alpha_\text{f} \nabla p + \alpha_\text{f} \nabla \cdot \boldsymbol{\tau} + \alpha_\text{f} \rho \boldsymbol{g} + \dot{\boldsymbol{S}}_u \quad 3.$$

$$\alpha_\text{f} \frac{\partial (\alpha_\text{f} \rho)}{\partial t} + \nabla \cdot \alpha_\text{f} \rho \boldsymbol{u}_\text{f} = 0. \quad 4.$$

The pressure is not directly solved for using the continuity equation (Equation 4) but is instead iterated using a pressure equation to enforce continuity, and the shear stress tensor $\boldsymbol{\tau}$ is given using a Newtonian viscosity ansatz or more sophisticated closure. This formulation of the Navier-Stokes equations, referred to in the literature as Model A, includes the fluid volume fraction $\alpha_\text{f}$ and the momentum exchange term $\dot{\boldsymbol{S}}_u$ that represent the presence of a Lagrangian phase. The other formulation, Model B, considers pressure to be attributed to the fluid phase, in contrast to Model A, which assumes a shared pressure among both phases. Consequently, the pressure gradient term in Model B reads $-\nabla \cdot p$, and the shear stress term, $\nabla \cdot \boldsymbol{\tau}$. This also causes the interaction forces to be summed up over the total control cell volume $V_\text{cell}$ in Model A and the fluid volume $\alpha_\text{f} V_\text{cell}$ in Model B, respectively. The forces involved include drag force, pressure gradient force, viscous force, and virtual mass and Basset forces in liquid–solid systems and the Saffmann shear lift force and Magnus force in the case of rotating particles. Although all of these forces may be present in any given physical system, their contribution might be negligible in modeling and thus can be avoided to reduce computational demand.

**2.1.4. Mapping procedures and numerical treatment of coupling.** The issue of solids-phase volume fraction calculation and mapping of properties from the discrete to the continuous phase is approached in several ways. The most popular is the iteration over all particles present in the cell and averaging/summing up their respective values, for example, the explicit heat flux source term from particles to fluid:

$$\dot{Q}_{\text{p}\to\text{f}} = \frac{\sum_{\text{particle } i \text{ in cell}} \dot{Q}_{\text{p}\to\text{f},i}}{V_\text{cell}}. \quad 5.$$

This very simplistic approach has the advantage of being very numerically efficient but introduces issues with fine grid cells and inaccuracies at cell boundaries. Thus, a decomposition of the particles into a cloud of $N$ subpoints with a numerical weight $\phi_{i,j}$ may be performed:

$$\dot{Q}_{\text{p}\to\text{f}} = \frac{\sum_{\text{particle } i \text{ in cell}} \sum_{\text{subpoint } j \text{ of particle } i} \phi_{i,j} \, \dot{Q}_{\text{p}\to\text{f},i}}{V_\text{cell}}, \quad 6.$$

with the weights for each particle $i$ summing to unity:

$$1 = \sum_{\text{subpoint } j \text{ of particle } i} \phi_{i,j}. \quad 7.$$

The added computational demand lies in associating the subpoints with grid cells—a process that is somewhat expensive in nonhexahedral grids. The choice in the position of subpoints, as well as the choice in weighting, leads to a variety of options for the end user or developer. The problem of numerical instability owing to particles covering entire cells or very large source terms may be addressed via a diffusion approach introduced by Pirker et al. (12), in which the corresponding source terms are smeared out using an implicit diffusion equation.

Coupled quantities like momentum, heat, and mass transfer are solved by alternating the solution of the flow field and the particle motion. Coupling itself takes place by adding source terms to differential equations that are integrated for each particle and to the continuous-phase transport equations. The source terms owing to momentum, heat, and mass rate laws can be treated in either an explicit or implicit manner for the discrete elements and the continuum (4).

**2.1.5. Drag coupling closures.** The most prominent problem with unresolved CFD-DEM is the closure for momentum exchange, i.e., the previously mentioned set of forces that are commonly modeled between particle and fluid. Of special importance is the drag force,

$$\boldsymbol{F}_{\text{drag}} = \frac{\pi}{6} d_{\text{p}} \frac{\beta}{\alpha_{\text{p}}(1-\alpha_{\text{p}})} (\boldsymbol{U}_{\text{f}} - \boldsymbol{U}_{\text{p}}), \qquad 8.$$

that is provided by experiment- or simulation-derived correlations. The momentum exchange coefficient $\beta_i$ aims to capture the highly complex hydrodynamics of momentum exchange depending on, at least, the particle Reynolds number $\text{Re}_{\text{p}}$ and, in general, the solids volume fraction in the vicinity of the particle. The most common correlation is that of Gidaspow (13), which uses the empirical Ergun correlation (14), as formulated by Beetstra (15),

$$\beta = 150 \frac{\mu_{\text{f}}}{d_{\text{p}}^2} \frac{\alpha_{\text{p}}^2}{(1-\alpha_{\text{p}})} + 1.75 \frac{\mu_{\text{f}}}{d_{\text{p}}^2} \frac{\alpha_{\text{p}}}{1-\alpha_{\text{p}}} \text{Re}_{\text{p}}, \qquad 9.$$

for flow below the minimum fluidization velocity and switches to the correlation of Wen & Yu (16, 17):

$$\beta = \begin{cases} \dfrac{18\ \mu_{\text{f}} \alpha_{\text{p}} (1-\alpha_{\text{p}}) (1-\alpha_{\text{p}})^{-3.65} (1 + 0.15\ \text{Re}^{0.687})}{d_p^2} & \text{Re}_{\text{p}} < 1,000 \\ \dfrac{0.33\ \mu_{\text{f}} \alpha_{\text{p}} (1-\alpha_{\text{p}}) \varepsilon^{-3.65}}{d_{\text{p}}^2} & \text{Re}_{\text{p}} > 1,000 \end{cases}. \qquad 10.$$

Both underlying relationships were derived from experimental investigations that have their uncertainties. Hill et al. (18), Beetstra et al. (19), Tenneti et al. (20), and Tang et al. (21), among many others, have applied the lattice Boltzmann and immersed boundary CFD-DEM methods to successively more complex particle flow scenarios to derive correlations between drag force and flow conditions—at first only for static arrays of spheres for low Reynolds numbers, then increasing the range of Reynolds numbers, and finally allowing the particles to move. Nonetheless, calibration of the drag force for real systems is required to match the minimum fluidization point, owing to the influence of surface roughness (22). In the case of nonspherical particles, more sophisticated drag laws must be used, for example, the one by Ganser (23), which considers the surface area of the particle, projected into the direction of the flow, or the one by Hölzer & Sommerfeld (24, 25), which also considers the chord length in the flow direction.

**2.1.6. Turbulence modeling.** The accurate representation of turbulent flows requires turbulence modeling for all practical intents and purposes. For the fluid phase, turbulent viscosity/Reynolds-averaged Navier–Stokes models like the k-ε or k-ω models are used, which solve

additional differential equations for the generation, transport, and dissipation of the turbulent kinetic energy and increase the viscosity depending on these quantities. As such, the effect of turbulence on averaged flow is captured without resolving the small length scales. Less often, large-eddy simulations are performed, in which eddies larger than a filtering criterion are resolved, and the effect of those eddies occurring on smaller length scales is modeled using an isotropic model like k-ε. In both cases, the effect on particles can be modeled stochastically by using the time spent in an eddy and the turbulent velocity fluctuation, both of which depend on the turbulent kinetic energy.

## 2.2. Coarse-Graining Techniques

Coarse-graining techniques aim to lower computational cost by reducing the overall spatial/temporal resolution of the fluid part and/or the particle part of the simulation while preserving macroscopic quantities and the overall temporal evolution of the system.

**2.2.1. Particle coarsening.** Owing to the computational cost of modeling the collision dynamics of every single grain in a granular system, particle coarsening (*a*) reduces the number of particles that must be tracked, so larger apparatuses and/or finer particles can be simulated, and (*b*) extends the process time that can be simulated by permitting a larger time step.

This makes particle coarsening nearly unavoidable when dealing with industrial-scale apparatuses. In the literature, such collectives of particles with identical properties are referred to as parcels. Most commonly, particles are enlarged by a factor of $\delta$, which decreases the number of particles by a factor of $\delta^3$ and increases the permittable time step by approximately a factor of $\delta$, as a rule of thumb. The DEM contact model coefficients are modified to preserve the bulk behavior by either using an a priori approach, e.g., by using the approach of Bierwisch et al. (26) or Benyahia & Galvin (27), or calibrating in a way that allows the macroscopic behavior of fine, real particles to be represented with larger numerical parcels (28).

Particle coarsening requires physical models to base their calculations on single-particle values (e.g., surface area) and then scale source terms with a factor $\delta^3$ to consider the number of primary particles per parcel, according to Radl et al. (29), or in other manners that are appropriate to the exact coarsening criteria that were chosen, e.g., for use with liquid–solid systems (30). The use of particle coarsening techniques introduces the need to coarsen the CFD or coupling grid, and to allow for accurate mapping and applicable phase fraction calculations.

**2.2.2. Fluid coarsening.** Coarser grids induce loss of local structure representation. The loss of sharp boundaries of, e.g., the edges of particle clusters induces the overestimation of drag force on particles. To correct for this, drag law corrections have been developed by performing simulations in which particles can swarm in a periodic box with gravity and a preset pressure differential for various Froude numbers and solids volume fractions on both refined and coarse grids (31). A different class of drag models, named energy-minimization multiscale models (32), aims to tackle this problem by correlating the fraction of particles that will cluster up to a certain size in each cell with the flow situation and, possibly, geometric parameters (i.e., distance to a wall) to predict the net drag force that will act on the particles. This is of interest in the context of industrial-scale fluidized beds, where applications of both fluid and particle coarsening are inevitable. An alternative to these kinds of models are the filtered drag models (31, 33). These offer a correction to regular drag laws and are obtained by performing simulations of particles falling in a fluid on successively coarser grids for different flow conditions and solids-phase fractions.

## 2.3. Thermochemical Modeling

Beyond pure particle and fluid dynamics, heat and mass transfer processes, as well as chemical reactions in the particle interior, the surface, and the gas phase, are of practical interest.

**2.3.1. Heat and mass transfer modeling.** Heat and mass transfer equations take a similar form. The transport of the mass fraction of a species $y_m$ can be described using

$$\frac{\partial \alpha_f \rho y_m}{\partial t} + \nabla \cdot \alpha_f \rho \boldsymbol{u}_f y_m = D_{y_m} \Delta \rho y_m + \dot{S}_{\text{particles},y_m} + \dot{S}_{\text{reactions},y_m} \quad 11.$$

under the condition of $\sum_{\text{species } m} y_m = 1$, where the latter condition can be resolved by either solving the transport equations for all species but one and explicitly calculating the remaining one or solving all transport equations and rescaling $y_m := y_m / \sum_{\text{species } k} y_k$.

The source/sink term $\dot{S}_{\text{particles},y_m}$ represents the link to the particle phase and considers the fluid-phase material that is exchanged with the particle, be it reaction products from internal or surface reactions, deposition onto the particle, or evaporation/devolatilization. The other source term, $\dot{S}_{\text{reactions},y_m}$, represents the contribution of the gas-phase chemical conversion.

The total energy equation takes the form of

$$\frac{\partial \alpha_f \rho (\, e_f + |||\boldsymbol{u}_f|^2/2)}{\partial t} + \nabla \cdot \alpha_f \rho \boldsymbol{u}_f (\, e_f + ||\boldsymbol{u}_f||^2/2) = \nabla \cdot \frac{\alpha_f \rho \kappa}{C_f} \nabla e_f + \dot{S}_{\text{particles},e} + \dot{S}_{\text{reactions},e}, \quad 12.$$

with terms due to compression/work omitted here. Here, $\dot{S}_{\text{particles},e}$ and $\dot{S}_{\text{reactions},e}$ are the source terms owing to heat transfer to/from the particles and gas-phase reactions, respectively, that are commonly treated via explicit–implicit splitting.

**2.3.2. Surface reactions, devolatilization, and gas-phase reactions.** Exchange of species between the particle phase and the fluid phase can occur owing to surface reactions and devolatilization or evaporation/vaporization of material. Both surface reactions and devolatilization are commonly treated with a kinetic/diffusion-limited rate model, e.g., for olefin polymerization (34), combustion (35), or gasification (36). Further complexity, as in the case of particle matter combustion, may be modeled using a shrinking core model that can consider the diffusion limiting introduced by the ash layers. These reaction rates are used to calculate source/sink terms for species transport equations in both the fluid phase and the particles. Gas-phase reactions are modeled independent of the presence of particles. Zhong et al. (37) provide a much more expansive treatment of this subject matter.

## 2.4. Liquid-Phase/Multiphase Treatment

Many apparatuses involve discrete particles and two or more fluid phases, especially those used for separation. The fluid phases are typically immiscible and require further modeling, such as the popular volume-of-fluid (VOF) method to preserve sharp interfaces. Sun & Sakai (38) formulated the corresponding flow equations using a color function $\phi$ that represents the fraction of either continuous phase and solved an advection equation,

$$\frac{\partial \phi}{\partial t} + \boldsymbol{u}_f \cdot \nabla \phi = 0, \quad 13.$$

that tracks the motion of the interface. The flow equations include a momentum source term representing the surface tension. The lumped fluid-phase density is calculated as a linear combination of the density of the constituent phases. Consequently, particles experience an additional

surface tension force. A particle encountering the interface of a bubble will experience a pressure jump, which will cause the surface tension to be balanced by the resulting pressure gradient force, effectively trapping the particle at the interface, as any displacement will result in a force toward the interface.

## 3. APPLICATIONS OF CFD-DEM TO DIFFERENT APPARATUS TYPES

### 3.1. Classification and Separation

The classification or separation of particles according to properties like size, shape, and density is often performed using a liquid or gas phase. This can include, e.g., screens (39, 40), gas or hydrocyclones (41–43), sorting machines (44, 45), flotation columns, and vessels (46–48). Coupled CFD-DEM simulations have been widely used for the microscale modeling of such processes in recent years.

In some of these investigations, the basic formulation of CFD-DEM, as described above, was applied (39, 49), involving only a particle and a single fluid phase. More advanced strategies are applied when more complex separation systems are concerned: Fernández & Nirschl (50) and Chu et al. (42) used the VOF model to consider a mixture of solid, liquid, and gas phases. In the first stage, the VOF was applied to model the interaction between slurry and air, without consideration of particles. The DEM was applied only in the second stage to consider particulate material. Regarding particle shape, most studies analyzed the separation or segregation of spherical particles (49, 51, 52). A significantly smaller fraction of contributions focused on classifying nonspherical or irregularly shaped objects (39, 45, 53). One of the main challenges here is properly describing the interaction between fluid and nonspherical particles, as described previously. For example, El-Emam et al. (53) used drag force correlation, proposed by Ganser (23), for the separation of seeds and leaves, and Pieper et al. (45) used the correlation derived by Hölzer & Sommerfeld (25) for slightly irregular peppercorns.

Chen et al. (46) contrasted the application of CFD-DEM to flotation with TFMs of flotation: They simulated a dissolved air flotation tank and described the air as a set of Lagrangian bubbles with an adapted contact potential and random-walk turbulence modeling. The CFD-DEM simulation failed to correctly reproduce the air distribution within this system, indicating that modeling of the dispersed-air (bubbly) phase using Lagrangian elements in that way is not yet a viable choice. Liu & Schwarz (48) first investigated modeling the interaction between bubbly flows and fine particles suspended in the liquid phase using CFD-DEM-VOF; they validated their model based on correct reproduction of particle collision efficiencies in a quiescent fluid. On this basis, they went on to study the dependence of drag and bubble–particle collision efficiency on turbulence and wall influences on the microscale using (CFD-)DEM-VOF and used the resulting model coefficients in macroscale homogeneous-phase CFD simulation to derive overall flotation rates of the simulated system (47). Wang et al. (54) presented a more comprehensive overview of other methods to assess flotation processes.

Both one- and two-way coupling can be employed: Particle influence on the fluid phase is neglected owing to the low solid concentration or to decrease computational effort (42, 45). Fernández & Nirschl (50) applied a slightly modified coupling scheme, considering the influence of particles on the fluid but only as a momentum sink term. The volume occupied by particles was neglected in the continuity and momentum conservation equations.

As mentioned above, the selection of the appropriate turbulence model has a decisive influence in CFD-DEM simulation results. The standard k-ε model is widely used for modeling comparatively simple flows, as in the case of an optical belt sorter (45). Use of this model for systems with high swirling turbulence, such as cyclone separators and those that use centrifugal forces to

induce sedimentation, can lead to incorrect results. Instead, more sophisticated models, like the k-ε renormalization group model (50, 53) or Reynolds stress model (RSM), are used (41, 43, 51, 55).

**3.1.1. General remarks.** Simplifications range from ignoring the presence of solid particles (50) to modeling particles with an artificially lowered Young's modulus (52). Despite that, CFD-DEM is an effective approach that can be used as a stand-alone tool or in combination with other methods and allows us to clarify different aspects related to the classification and separation of solid particles in a fluid field. However, this approach cannot be accurately used for particle collectives with very wide size distributions. The main drawback is the nature of unresolved CFD-DEM coupling, whereby a CFD mesh cell must be larger than the largest particle. In this case, the slipstream effect, in which small particles enter in the wake of larger ones, will be totally neglected, and the drag force on small particles will be overpredicted.

## 3.2. Fluidized Beds for Particle Formation

Nowadays, fluidized beds are widely applied in several industrial fields, e.g., chemical production, energy generation, and pharmaceutical and food industries. In a fluidized bed vessel, an upward gas flow is introduced at the bottom through a distributor plate. The solid is entrained by the gas flow and thus fluidized. The outward appearance is that of a bubbling fluid owing to bypass gas that rises in the form of bubbles. The intense particle movement owing to bubbling in fluidized beds enables high heat, mass, and momentum transfer rates, which make this apparatus highly suitable for particle formation, e.g., agglomeration, granulation, and coating.

Coating commonly refers to the application of layers of material to the entirety of the particle surface to protect or contain its material without adding much substance to the particle. Granulation, more precisely called layering granulation, refers to the substantial addition of material to a particle's surface to increase its diameter while creating structures that aid its purpose, i.e., porous structures for rapid dissolution or dense layers for high strength. Agglomeration, also called agglomerating granulation, refers to increasing particle size by having smaller, primary particles stick together and sinter together. All three will take place simultaneously in a granulator, with only one of these mechanisms being desired to yield a given product. Thus, controlling these is one of the main challenges in using fluidized beds for particle formation.

Along with the classical fluidized bed with the distributor plate ranging over the whole cross-sectional area, similar apparatuses have been developed with advantages for certain applications. In spouted beds, the gas enters the process chamber via a tube or a slit, which results in higher gas and particle velocities and allows the fluidization of particles, which are often difficult to handle in fluidized beds owing to their surface properties or size. In a fluidized bed with a centered, vertically installed draft tube (Wurster coater), the wetting and drying zones are separated, reducing the risk of agglomeration (56).

In the early 1990s, Tsuji et al. (3) performed one of the first attempts to apply CFD and DEM to a pseudo-2D fluidized bed. The authors observed a qualitative agreement between fluidization and mixing behavior with experimental data and quantitative agreement of the frequency of pressure fluctuations. Nevertheless, deviations between experiments and simulations occurred in the scale of circulations and in the amplitude of pressure fluctuations. In the following years, many other authors applied CFD-DEM simulations to 2D or 3D apparatuses and compared the resulting flow, mixing, and bubbling patterns with experimental data (57–67).

In addition, some researchers have undertaken special applications of fluidized beds, e.g., Wang et al.'s (68) investigation of the effects of sound fields on fluidization behavior, in which they integrated a sound force into their numerical model. They found that the sound field enhances the

fluidizability of cohesive particles, whereby the effect depends on the sound pressure level and the sound field frequency. Limtrakul et al. (69) investigated the flow behavior in a vibrated fluidized bed used for fluidization of cohesive particles, modeled using Hamaker's formulation of the van der Waals force. They applied a vibrational force into their CFD-DEM model by enforcing a sinusoidal vertical vibration on the gas distributor and the walls of the fluidized bed. They found higher-amplitude and -frequency vibration to result in a more intense fluidization and better mixing. The results were validated only by indirect comparison to experiments. Zhenghua et al. (70) simulated the flow behavior of magnetizable particles in a 2D-gradient magnetically assisted bubbling fluidized bed. The authors included a magnetic force resulting from the interaction of the external uniform field and nonuniform fields of the magnetized particles in their model. Pei et al. (71) applied CFD-DEM with a capacitor model for modeling contact electrification. For the investigated fluidized bed case, they showed that the charge is initially generated in the regions near the walls and then propagates into the entire granular bed, induced by particle mixing and particle–particle collisions. Namdarkedenji et al. (72) studied the effect of flow pulsation on fluidization degree and found the pulsation to decrease the gas–solid interaction force but to increase the contact force between particles.

Along with the classical fluidized beds, flow behavior in related apparatuses has been part of numerical investigations using the CFD-DEM approach since the 2000s. For example, Kawaguchi et al. (73) found high qualitative consistency between their simulation data and experimental data from the literature for their cylindrical spouted bed, even though deviations in the particle velocity distribution occurred. Other authors (e.g., 11, 74–80) also performed simulations of hydrodynamics in a spouted or spout-fluid bed and compared results with experimental data. In 2006, Nakamura & Watano (81) investigated a rotating fluidized bed using the CFD-DEM approach. The authors found high agreement between bubble formation, eruption, and particle circulation with experimental data from high-speed camera recordings. In addition, Nakamura et al. (82) compared the degree of particle mixing with images recorded by a high-speed camera and found strong agreement between numerical and experimental data. Neuwirth et al. (83) simulated the granular flow in a rotor granulator and determined the influence of different process parameters on particle and collision dynamics. Experimental data obtained via a magnetic particle tracking system validated the model. Deb & Tafti (84, 85) simulated a fluidized bed with multiple jets and a spouted bed with multiple jets, respectively.

Early numerical investigations on fluidized beds and related apparatuses focused mostly on monodisperse particle systems. However, Feng et al. (86) and Tagami et al. (87), for example, observed segregation effects when investigating binary mixtures and polydisperse particle systems, respectively. Olaofe et al. (88) predicted segregation effects observed in experiments by applying the drag model derived from DNS simulations by Beetstra et al. (19) for polydisperse systems. However, deviations occurred when the bed height exceeded the bed width. Hilton et al. (89) investigated nonspherical particles in their CFD-DEM simulations by introducing a new pressure gradient force Navier–Stokes formulation and by calculating the drag force according to Hölzer & Sommerfeld (24), accounting for nonsphericity. They found a strong effect of nonsphericity on the flow behavior and deviations from the Ergun equation. Zhou et al. (90) applied Hölzer & Sommerfeld's (24) correlation and investigated the effect of ellipsoidal particles with different aspect ratios on fluidization behavior. They found that the particle orientation of ellipsoidal particles is not random, as it is for spheres. Ma et al. (91) studied the fluidization of rodlike particles in a fluidized bed. The rodlike particles were modeled by superellipsoids with different aspect ratios.

Along with hydrodynamic investigations, simulations considering agglomeration phenomena or applications such as granulation or coating owing to liquid binder injection have been researched. Collision frequencies and acting forces have been extracted from simulations to account

for agglomeration probability or particle stress, and effects of liquid–particle interactions have been studied. Kuwagi & Horio (92) investigated a fluidized bed with cohesive particles and detected agglomerate formation if the cohesive force exceeded the maximum repulsive force during particle contact. They found agglomerates to be formed in the bubble wake region and agglomerate breakage to occur mostly in the bubble upper region. Kuwagi et al. (93) extended a CFD-DEM model via tangential lubrication effects caused by liquid bridges between particles. They found the particles to move more actively in the whole bed and adhesion of particles to the walls to be reduced. Fries et al. (94) compared two different granulator configurations (top-spray fluidized bed and Wurster coater) by calculating the residence time distribution of the particles in the spray zone and estimating the homogeneity of the liquid distribution, even though no liquid phase had been injected. Fries et al. (95) extended their investigations by calculating agglomeration probability, breakage and growth rate, and agglomerate strength based on particle motion, collision dynamics, and collision frequencies. They compared three different apparatuses, namely, top-spray fluidized bed, Wurster coater, and spouted bed, and found the most stable and redispersable agglomerates of amorphous dextrose syrup to be produced with the Wurster coater device. Li et al. (96) performed similar investigations, determining the residence time distributions of different-sized particles in the spray zone of a Wurster fluid bed. They observed that large particles receive more coating per unit area per pass through the spray zone, as they have a longer residence time, but also travel through the spray zone less frequently than small particles. Azmir et al. (97) simulated the drying of food grain in a fluidized bed. They modeled water evaporation from the particles similar to a surface chemical reaction, which required fewer model parameters. Owing to the low particle moisture content in the studied cases, the authors assumed all water to be adsorbed and thus did not consider liquid bridges and capillary forces. They found the average drying rate and moisture content to be consistent with experimental data. Goldschmidt et al. (98) first attempted to simulate particle–droplet interactions in 2003. Besides the particles themselves, injection of melted binder droplets was considered as an additional discrete element. They considered a wide range of interaction scenarios in their model. These included the impact of particles onto droplets, the subsequent transfer of liquid onto the surface, and particle growth. Interaction among particles was modified to distinguish among rebound and agglomeration scenarios that are dependent on the wetting state of particles and their velocities. Layering granulation dominated in comparison to agglomeration, and particle segregation was observed. Nevertheless, owing to the high computational effort, the study was limited to a 2D fluidized bed with only 50,000 primary particles and unrealistically large droplet diameters of 100 μm. Furthermore, no heat or mass transfer was calculated. Link et al. (99) integrated droplet injection into a pseudo-2D spout-fluid bed for granulation applications. Along with some other simplifications, particle growth was assumed to consist solely of the one-by-one mergers of droplets with particles. When a droplet hits a particle, its mass and momentum are directly transferred to the particle. They found particle growth rate and particle size distribution depended on the projected surface area of the particles and on the position of the particle relative to the spout. Nevertheless, no validation with experimental data was performed, and the model contained several simplifications neglecting heat and mass transfer effects. Van Buijtenen et al. (100) extended Link et al.'s (99) model by incorporating the full equation of motion of the droplets, two-way coupling of the drag between the droplets and the gas phase, and moisture evaporation from the particle surface. They considered liquid cohesion by reducing the restitution coefficient in regions that were assumed to be wet. The model nevertheless included simplifications, as the mass and energy balances of the gas phase were not solved, and crystallization of the deposited granulate solution was not considered. Sutkar et al. (101) then further extended van Buijtenen et al.'s (100) model to account for heat and mass transfer in the spout-fluid bed with liquid injection. The net effect arising due to various forces at particle–droplet

impact was reproduced by modeling the wet restitution coefficient. The implementation of the heat and mass transfer was verified by conducting various tests and subsequent comparison of the computational results with analytical solutions. Simulation results of the spout-fluid bed were found to be in good agreement with data from infrared temperature measurements, even though, e.g., viscous forces between wetted contacting particles were not simulated. Liu et al. (102) applied a CFD-DEM model to account for agglomeration and breakage phenomena in a fluidized bed of nanoparticles. They included an adhesive contact model with the ability to model the contact and bounce/stick between elastic–plastic and cohesive particles.

To account for agglomeration, granulation, and breakage phenomena in fluidized beds, a hybrid CFD-DEM-PBM model that incorporates a population balance algorithm into CFD-DEM simulations has emerged as a popular tool to tackle the timescale separation between particle dynamics and growth/agglomeration/breakage. The general idea is to transfer the hydrodynamics of the regarded process calculated with CFD-DEM to PBM to simulate the global process on the macroscale. For example, Dosta et al. (103) applied this approach to calculate breakage phenomena in a fluidized bed, and several authors, e.g., Dosta et al. (104), Sen et al. (105), and Tamrakar & Ramachandran (106), applied it to fluidized bed granulation processes. Heinrich et al. (107) investigated the coating process in a Wurster fluidized bed via a multi-scale simulation approach combining CFD, DEM, and PBM. The authors found the gap distance of the Wurster tube and the distributor plate to have a significant influence on particle circulation and on residence time in the spray zone. In general, the multi-scale approach aids in determining the influence of critical process parameters, e.g., air flow rate and binder spray rate, on macroscopic process performance.

The use of CFD-DEM for the design of particle formation apparatuses like fluidized bed granulators can be considered very mature in the aspect of pure hydrodynamics and heat transfer when dry, coarse particles and small apparatuses are to be considered. Larger apparatuses or very fine particles still touch the limit of computational capacity available and warrant the use of either apparatus or particle scaling. When using scaling, the modeling of liquid bridge forces poses a challenge to researchers, as the applicability of the models is still strictly limited to the contact of single particles. Treating fine powders demands the application of both scaling laws and drag corrections. More complicated processes, such as fine powder agglomeration or drying, are therefore still within the realm of research rather than reliable application. Similarly, the use of CFD-DEM for engineering the actual product of the process itself rather than the process stability is rare and still an area of active research.

### 3.3. Fluidized Beds for Chemical Reactors and Energy Technology

Along with its application in fluidized bed apparatuses for particle formation, the CFD-DEM method is used for chemical reaction engineering and energy technology, e.g., combustion, cracking, and gasification, owing to its excellent gas–solid contacting, good heat transfer, ease of solids handling, and increased resilience toward hot spots even with exothermal reactions (108). These processes often involve high temperatures and thus require the integration of heat transfer in modeling and simulation. In addition, chemical reaction rates must be considered.

Kaneko et al. (109) performed one of the first attempts to simulate chemo-thermal processes in fluidized beds using the CFD-DEM method when simulating a fluidized bed reactor for polyolefin production. The authors integrated the energy balance and reaction rate into the model and estimated the heat transfer from the particles to the gas phase using the Ranz–Marshall correlation. They found that hot-spot formation in the bed is often caused by a large stable particle revolution flow. Kuwagi et al. (110) performed CFD-DEM simulations of metallic solid bridging particles in a fluidized bed at high temperature. Surface-diffusion mechanisms, including

the effect of surface roughness of small grains on the particles' surface area, were integrated to model the solid bridging force. Zhou et al. (111) simulated heavy-metal vaporization dynamics. They extended the bubbling fluidized bed model with a cadmium chloride vaporization model and integrated the $CdCl_2$ transport equation into the gas flow. Comparison with experimental data showed strong agreement with the vaporization rate within the first 20 min. Later experiments showed a reduction in the vaporization rate owing to a possible chemical reaction between $CdCl_2$ and alumina, which was not integrated into the simulations and thus resulted in deviations. In another paper, Limtrakul et al. (112) simulated a spouted bed reactor for the decomposition of ozone on oxide catalyst. The reaction was assumed to be isothermal first-order irreversible heterogenous-catalytic. The simulated conversion results showed good agreement with experimental data from the literature at an absolute error of less than 5%. Czok et al. (113) investigated the thermal decomposition of triisobutylaluminum to produce aluminum on glass beads. The deposition reaction on the particles' surface was simulated not within the CFD-DEM simulations but in a postprocessing step, whereby it was assumed that the change in local precursor concentration due to reaction and the resulting change in number of gas molecules did not significantly influence the fluid mechanics. With this approach, the authors identified zones of insufficient mixing, as well as zones of possible agglomeration owing to excessive deposition.

Regarding the integration of heat transfer rates into CFD-DEM simulations of fluidized beds, Di Maio et al. (114) integrated three different approaches into a simulation framework for a fluidized bed and compared the heat transfer coefficient between a hot bed and an immersed probe with experimental data. The heat transfer based on a particle–particle transfer mechanism avoiding the use of particle contacts by using increased heat transfer to the gas phase best represented the real fluidized bed system. Zhou et al. (115) proposed introducing a correction factor to account for the use of a nonphysical Young's modulus and its influence on contact-based particle–particle heat conduction. Patil et al. (116) developed a CFD-DEM model including heat transfer, whereby for particle–particle heat transfer, the total heat or energy transfer during one collision is calculated and directly transferred as a packet of energy at the beginning of the collision. The unknown fitted gas-wall heat transfer coefficient was used to match experiment and simulation results with respect to bed cooling curves. Results were validated with experimental data from infrared/visual measurements. Wu et al. (117) investigated a fluid catalytic cracking process in a fluidized bed by means of CFD-DEM simulations. The hydrodynamic model was extended by a model to describe the heat transfer between particles and between a particle and a gas phase, by a model for catalyst deactivation, and by a model for gas-phase reactions. They used a 4-lump kinetic model to describe the chemical reactions, whereby the temperature dependence was described by Arrhenius expressions. They calculated catalytic activity using the recorded residence time of the catalytic particles. In their simulations of a methanol-to-olefins process, Zhuang et al. (118) accounted for both heat transfer and lumped kinetics in the gas phase. Simulations were performed in two stages: In the first stage, the flow field was simulated without the methanol-to-olefins reaction. When a fully fluidized bed was obtained under cold-flow conditions, DEM and the submodels for heat transfer and reaction rates were incorporated into the simulations. Ku et al. (119) simulated biomass gasification with steam in a fluidized bed. They expressed the pyrolysis compositions released from biomass using an equilibrium equation and elemental conservation analysis of the involved substances and modeled the devolatilization rate using a single-step first-order Arrhenius reaction. Using this approach, they analyzed the effects of different operating conditions on the gasification performance; higher temperatures were found to be favorable for the products in endothermic reactions. Li et al. (120) performed CFD-DEM simulations of a fluidized bed methanation reactor. The authors integrated a new local-structure-dependent drag model and modified reaction kinetics for the CO methanation

and the water–gas shift. They verified their assumption of isothermal flow conditions in the investigated lab-scale fluidized bed by solving the energy equations for the gas phase and seeing little difference. Bellan et al. (121) investigated a fluidized bed reactor for solar gasification. The authors integrated a discrete ordinate radiation model to solve the radiative transfer equation. El-Sayed & Noseir (35) applied the CFD-DEM approach to the combustion process of sesame and broad bean stalks in a pilot-scale bubbling fluidized bed combustor. They considered the mass and heat exchange and homogeneous and heterogeneous chemistry between the two phases and of the gas species, whereby a finite-rate/eddy-dissipation model was selected for the gas-phase reaction. The authors found good agreement between their simulation results and experimental data at a relative error of gas phase composition of less than 11% and axial temperature of less than 15%.

Overall, the application of the CFD-DEM method for energy technology and chemical conversion is very mature, but less prominent due to other competing methods like MP-PIC and TFM. The special demands and challenges of these fields lie in the very small particles and large plants, along with a focus on reaction modeling on both particle surfaces and the gas phase. The depiction of actual contact mechanics usually matters very little in comparison—a factor that reduces the need for CFD-DEM except for in apparatuses with both fluidized and densely packed regions, like spouted beds.

### 3.4. Comminution Units

To perform milling of granular materials and to reach a desired size distribution, an additional fluid phase is often essential. In most cases, the fluid plays a decisive role in the process behavior. It is used for dispersion or for material transport, such as in ball mills, where source material and grinding balls are dispersed in a liquid medium. In other cases, the fluid phase is used to give particles the necessary kinetic energy prior to their impact, as in jet mills. Consequently, proper simulation of such processes requires consideration of not only the solid but also the fluid phase. Thus, in recent years, the CFD-DEM approach has been used for various apparatuses, from ball mills to jet mills. All CFD-DEM applications for milling process modeling can be generally classified into three main levels, depending on how the breakage process is considered:

- No particle breakage: In this case, CFD-DEM simulations provide trajectories of particles, residence time distribution, or their concentration in different regions (122, 123).
- Breakage during postprocessing: Statistics about particle–particle and particle–wall collisions are collected and used to simulate breakage in additional submodels (103, 124, 125).
- Direct simulation of breakage: When a predefined breakage condition is reached, a large particle is destroyed, and new, smaller fragments appear (126, 127).

A wide variety of applications can be found for both solid–liquid and gas–solid milling. In most cases, two-way coupling is employed; however, for dilute gas–solid systems, one-way coupling is also often applied.

Using liquid as the fluid phase, Jayasundara et al. (122) applied CFD-DEM to model particle flow in a high-speed stirred mill. Their simulation results were in reasonable agreement with experimental data with respect to particle dynamics. However, no breakage was considered, nor impact statistics analyzed. To analyze breakage behavior of grinded material in a wet ball mill, Kushimoto et al. (127) investigated aggregate breakage. The aggregates were represented as sets of primary particles connected with bonds. Such an approach allowed them to reproduce the breakage process directly during the CFD-DEM simulation and not only during the postprocessing step, thereby accounting for secondary breakage and the influence on flow.

With respect to gas–solid systems, many have analyzed the influence of the main process parameters on particle–particle or particle–wall collisional statistics (123, 128). To consider both breakage and fatigue behavior of particles, Brosh et al. (124) introduced a function to change particle properties and applied their proposed model to investigate jet-mill behavior. For modeling of a pulverization process, Takeuchi et al. (126) used a strategy employing direct simulation of particle breakage. If the impact stress exceeded the specific threshold strength, the old particle was replaced by smaller particles, representing breakage fragments.

A wide spectrum of apparatuses in the field of milling are seeing application of CFD-DEM, for both gas–solid and solid–liquid systems. In most cases, good agreement between experimental and numerical results can be obtained. However, detailed simulation of milling processes is still very challenging, because various effects take place on different time and length scales.

One of the main challenges is the consideration of particle breakage with DEM. Some authors, e.g., Takeuchi et al. (126) and Kushimoto et al. (127), consider breakage directly. However, such an approach involves very high computational effort. The incorporation of fragments leads to a drastic increase in the number of modeled objects, as well as a decrease in the simulation time step. Thus, in most cases, CFD-DEM calculations are used only as a source of information regarding stressing conditions, such as impact velocities or frequencies (124, 125). The actual modeling of the breakage takes place in submodels on higher hierarchical scales, where one- or multidimensional population balance models are often used. Such multiscale process treatment, in which the submodels from different time and length scales are coupled together, allows detailed process descriptions with limited computational effort (103, 129).

Generally, the state of DEM and CFD-DEM regarding comminution can be judged to be mature for the purpose of qualitatively evaluating the influence of geometry and operation parameter changes. Quantitative predictions about resulting fragment size distributions suffer from the general scale problem, as tracking fragments directly will require smaller time steps and increase computational cost. Indirect approaches fail if second-order effects appear. Micromechanical fracturing models furthermore demand calibration. Thus, we deem the quantitative description of comminution processes using CFD-DEM as an active area of research.

## 3.5. Filtration

Filtration is often applied in the chemical industry, agriculture, and environmental engineering. Different filter processes can be distinguished depending on the filter medium, process conditions, or acting forces, but all are based on the same principle: A heterogeneous mixture is poured over a filter membrane with pores of a given size. Particles larger than this size are retained, whereas smaller particles can cross the membrane. The fluid can permeate through the membrane, encountering flow resistance owing to the accumulation of particles and the constriction of flow through the pores.

In one of the first approaches to simulating filtration processes with CFD-DEM, Li & Marshall (130) simulated microparticle deposition on a cylindrical fiber in an array, considering the adhesive elastic contacts of the particles and the fiber. They found the particles tended to deposit in a narrow region along the fiber front near to the centerline owing to particle shadowing and high shear stresses. Nevertheless, the model did not consider porosity changes in the fibrous media and flow field after the particles were deposited. No fluid forces except the drag force, calculated using the Di Felice drag law, and torque were considered. Qian et al. (131) developed a model for simulating gas-flow characteristics within a fibrous medium and studied the influences of fiber structure and particle properties on the deposition and agglomeration characteristics in the filtration process. The 3D models of the fibrous media were reconstructed from scanning

electron microscopy data. They found the simulated filtration efficiencies to be consistent with calculated values of empirical correlations. Qian et al. (132) simulated gas–solid flow characteristics in fibrous media exposed to particle loading by using CFD-DEM, adopting the Hertz–Mindlin contact model, in the JKR-cohesion model variant, to accurately describe the interactions between particles and filter material. They used a two-way coupling approach considering the interactions of the particle–fluid, particle–particle, and particle-filter material. Dong et al. (133) performed a numerical study on the deposition process of submicron particles in collision with a single cylindrical fiber. They found that the deposition can be divided into two stages: particle deposition on the surface of the fiber and subsequent growth of formed agglomerates to branched dendrites. Recently, Naukkarinen et al. (134) investigated the hydrodynamics of a combined ion-exchange membrane filtration unit used for wastewater treatment using the CFD-DEM approach. Li et al. (135) investigated a pressure filtration process and simulated the effect of solvent flow through a solids particle bed of glass beads. During pressure filtration, the cake thickness continuously increased with an increasing number of deposited particles. Their CFD-DEM model accounted for different solids properties, such as polydispersity and compressibility, as well as liquid properties, such as density and viscosity. The model was successfully validated by comparing the obtained cake resistance and filtrate flow data with experimental data.

Due to the often very fine particles that are to be modeled, usually only the microscale—comprising few fibers and pores—is modeled, and macroscopic filter coefficients are derived. These in turn, can be used in larger-scale simulations of actual filtration apparatuses. However, the state of the art in filtration unit design has not yet come to fully realize the advantages of the increasingly sophisticated methods that can cover a wide range of features, like the work of Li et al. (135). Whereas the CFD-DEM method can, as far as physical models are concerned, be considered mature for this purpose, due to insufficient development of multi-scale approaches, its industrial application cannot.

### 3.6. Bioreactors

A bioreactor is a vessel in which physiological conditions are carefully controlled to induce certain behavior in living cells, tissues, or organs (136). In most bioreactors, the biological phase is suspended in the liquid phase in the form of isolated cells, biological aggregates, or biofilm developed on carrier solids. In comparison to chemical reactions, the reaction rate depends not only on thermodynamic variables (temperature, pressure, composition) but also on the state of the microorganisms (137). Bioreactors can have different geometries and different inserts for aeration or stirring. Nevertheless, in all of them a certain shear stress is applied to the biological material. Detailed investigations of the applied stresses can be included in numerical investigations.

Morchain (137) compared the Euler approach with the Euler–Lagrangian approach for modeling bioreactors. He concluded that a three-phase Eulerian approach, consisting of a gaseous, a liquid, and a biological phase, is the best choice for simulating bioreactors, as transfer and reaction rates must be described correctly for the Lagrangian approach. Another challenge he identified is the huge number of particles in the system, as a volume fraction of 0.1%, approximately 1 g/L, corresponds to $10^{12}$ cells/cm$^3$. In addition, the liquid phase's concentration field must be modified owing to assimilation or excretion by the microorganisms, which poses another challenge.

Yamamoto et al. (138) investigated the suspension of cell colonies in bioreactors of stirring and orbiting shaking tanks. The authors modeled the cell colonies in a culture liquid as rigid spherical solid particles. The maximum shear stress acting on the particles in the stirring tank was higher than that on the particles in the orbital shaking tank, whereas the average shear stresses were comparable. Tan et al. (139) simulated a membrane-assisted fluidized bed reactor for ultrapure

hydrogen production. They extended the DEM model using gas species transport equations and studied the effect of hydrogen extraction in the micro reactor at various conditions. De Jong et al. (140) investigated a pseudo-2D fluidized bed membrane reactor 4 cm in width with flat membranes in the left and right walls via CFD-DEM and with a TFM approach. A prescribed influx boundary condition was applied to the membranes and the bottom distributor plate. Both models showed qualitative agreement with experimental data, but quantitative deviations occurred. Using the CFD-DEM approach, Hirche et al. (141) investigated an anaerobic fluidized bed membrane reactor with granular activated carbon particles as a scouring material. The authors investigated different reactor geometries, particle sizes, and inlet velocities and determined their influence on membrane fouling.

Due to the wide range of possible phenomena to which CFD-DEM could be applied, one must distinguish between a few cases to assess their maturity. Treating the cells or cell colonies as particles is most common, and using CFD-DEM to track both their internal state and the chemical conversion in the Eulerian phase takes advantage of the Lagrangian frame of reference but does not strictly require particle collision modeling and suffers from issues regarding timescale and particle number. This field can still be considered a field of active research. Rheological studies of entire apparatuses mostly choose a fluid-only approach, but a few studies have been set on deriving the influence of shear conditions on cells. Suspension of particles in bioreactors is usually well described and mature, benefitting from previous work for chemical reaction vessel engineering.

## 4. PERSPECTIVE AND FUTURE TRENDS

Use of the CFD-DEM method has been expanding continuously since its inception, and we expect it to continue to do so. Its robustness and adaptability to a wide variety of physical phenomena make it a worthwhile addition to the skill set of any researcher or engineer tasked with the design of solids processing apparatuses. We have identified the following areas as the most promising in which to conduct methodical research, apart from the pure application of the method and extension to more flow situations.

### 4.1. High-Performance Computing

One of the main limiting factors related to the use of CFD-DEM is the high computational effort involved, which, in most cases, is caused by the DEM. Owing to the small size and high stiffness of particles, the simulation time step of DEM is often two orders of magnitude smaller than the CFD step. To decrease computational time, different parallelization strategies have been developed recently (142, 143). Some are based on the use of distributed memory approaches using message-passing interfaces that allow execution on large clusters, shared memory approaches like threading to fully utilize multiprocessor architectures, or hybrid combinations of both (143). Others focus on the use of graphic processor units (GPUs) to parallelize DEM calculations (142). In the near future, we are expecting intensive research in this field, especially with respect to the use of modern computer architectures such as GPUs.

### 4.2. CFD-DEM as Part of Multiscale Calculations

CFD-DEM coupling is an effective approach that can be applied to investigate specific questions with respect to multiphase flows. This method can be applied only for relatively small time and length scales. To link the simulation results with the macroscopic production process or with final

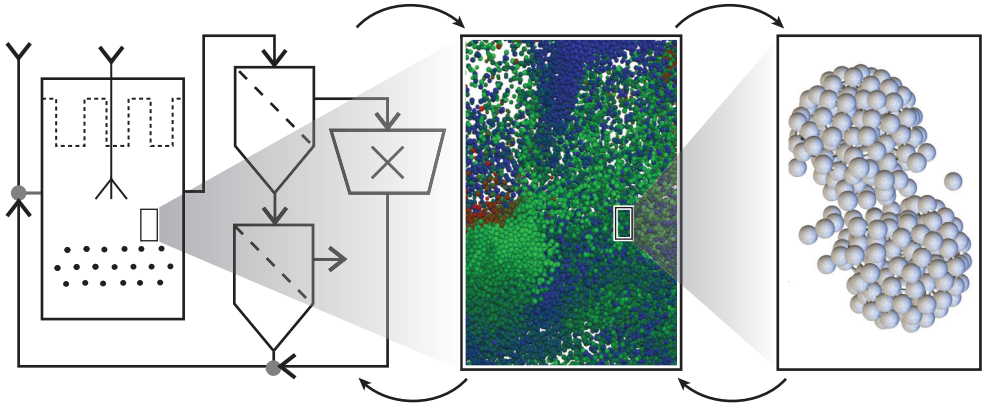

**Figure 2**

Usage of computational fluid dynamics–discrete element method (CFD-DEM) as part of multiscale calculations. Reprinted with permission from Reference 103; copyright 2013 American Chemical Society.

product properties, additional submodels are needed. Thus, in recent years, CFD-DEM has been used as part of multiscale simulation frameworks, where it has been coupled to models on other scales, such as bonded-particle models, population balance models, and flowsheet calculations (103, 107), as is schematically shown in **Figure 2**. We expect that future research in this field will focus on integrating CFD-DEM calculations into one simulation framework.

**4.2.1. Time extrapolation methods and data-driven modeling.** Owing to its high computational demand, the CFD-DEM approach cannot be used to directly model process behavior over long time spans. To ameliorate this problem, different extrapolation strategies have been developed: Their main idea is to use CFD-DEM simulation on short time intervals, on the order of seconds, to capture system characteristics and afterward extrapolate data for longer time intervals. This can include methods based on assumed repeated particle trajectories (104) or more advanced approaches like recurrence CFD (144), in which recurrent global flow fields are sampled, the pairwise similarity of different states is assessed, and tracer particles are moved based on remixed sequences of velocity and phase fraction fields. Lichtenegger (145) showed the sufficiency of this approach to capture dynamics over very long time spans, even using only local information. It has been used successfully for fluidized beds with heat transfer (146), spray coating in spouted beds (147), and heat transfer in a fluidized bed with a transient change in air velocity (148). It has the advantage of preserving physical intuition and state data over population-balance modeling, allowing us to stretch the applicability of a given sampled state of operation at speedups of approximately two orders of magnitude, all the while employing physical models that match those used in regular CFD-DEM. Recently, Pirker & Lichtenegger (149) developed a real-time-capable variant of this method based on transition patterns rather than Lagrangian tracers that shows great promise for model-based control, as displayed in their first proof of concept on a turbulent mixing chamber (150). We see a great future in this technology and would welcome further research in this area, as well as integration into general-purpose CFD codes.

## 4.3. Data-Driven Closures

An Achilles' heel of the CFD-DEM method is its need for closures for drag, heat, and mass transfer. A lot of information is lost regarding the arrangement of particles in both the derivation of

the drag correlation that traditionally depends primarily on the Reynolds number and the solids-phase fraction, as well as the application within the drag force calculation. Applying artificial neural networks to preserve some of the complexity of these flow situations provides one opportunity to alleviate this situation: He & Tafti (151) trained neural networks to correct the drag force depending on the relative position of surrounding particles to yield a more accurate drag prediction. Yan et al. (152) used a radial basis function neural network to capture the drag coefficient of nonspherical particles based on their sphericity but applied it only in TFM simulations. Jiang et al. (153) introduced a new way to filter corrections in coarse-grid TFM simulations to predict drift velocity below the grid scale, which ultimately affects the drag coefficient. Beck et al. (154) showed the applicability of neural networks as sophisticated closures in turbulence modeling (large-eddy simulations).

We are confident that more developments of this kind will have a big impact on simulation accuracy. One general concern, the sheer number of arithmetic operations that must be performed for a single evaluation of neural networks, is conquered via use of GPUs or specialized coprocessors designed for the execution of neural networks.

## DISCLOSURE STATEMENT

The authors are not aware of any affiliations, memberships, funding, or financial holdings that might be perceived as affecting the objectivity of this review.

## LITERATURE CITED


1. Merrow EW. 1986. *A quantitative assessment of R&D requirement for solids processing technology*. Rep., Rand Corp., Santa Monica, CA
2. Tsuji Y, Tanaka T, Ishida T. 1992. Lagrangian numerical simulation of plug flow of cohesionless particles in a horizontal pipe. *Powder Technol.* 71(3):239–50
3. Tsuji Y, Kawaguchi T, Tanaka T. 1993. Discrete particle simulation of two-dimensional fluidized bed. *Powder Technol.* 77(1):79–87
4. Radl S, Gonzales BC, Goniva C, Pirker S. 2014. *State of the art in mapping schemes for dilute and dense Euler-Lagrange simulations*. Presented at the 10th International Conference on Computation Fluid Dynamics in the Oil and Gas, Metallurgical and Process Industries, Trondheim, Norway
5. Snider DM. 2001. An incompressible three-dimensional multiphase particle-in-cell model for dense particle flows. *J. Comput. Phys.* 170(2):523–49
6. Snider DM, Clark SM, O'Rourke PJ. 2011. Eulerian-Lagrangian method for three-dimensional thermal reacting flow with application to coal gasifiers. *Chem. Eng. Sci.* 66(6):1285–95
7. Ding J, Gidaspow D. 1990. A bubbling fluidization model using kinetic theory of granular flow. *AIChE J.* 36(4):523–38
8. Chen P, Yuan Z, Chyang C-S, Zhuan F-X. 2011. Sawdust discharge rate from aerated hoppers. *Particuology* 9(3):306–13
9. Ozarkar SS, Yan X, Wang S, Milioli CC, Milioli FE, Sundaresan S. 2015. Validation of filtered two-fluid models for gas-particle flows against experimental data from bubbling fluidized bed. *Powder Technol.* 284:159–69
10. Gryczka O, Heinrich S, Deen NG, van Sint Annaland M, Kuipers JAM, et al. 2009. Characterization and CFD-modeling of the hydrodynamics of a prismatic spouted bed apparatus. *Chem. Eng. Sci.* 64(14):3352–75
11. Salikov V, Antonyuk S, Heinrich S, Sutkar VS, Deen NG, Kuipers JAM. 2015. Characterization and CFD-DEM modelling of a prismatic spouted bed. *Powder Technol.* 270:622–36
12. Pirker S, Kahrimanovic D, Goniva C. 2011. Improving the applicability of discrete phase simulations by smoothening their exchange fields. *Appl. Math. Model.* 35(5):2479–88

13. Gidaspow D. 2012. *Multiphase Flow and Fluidization. Continuum and Kinetic Theory Descriptions*. Cambridge, MA: Academic. 1st ed.
14. Ergun S. 1952. Fluid flow through packed columns. *Chem. Eng. Prog.* 48:89–94
15. Beetstra R. 2005. *Drag force in random arrays of mono- and bidisperse spheres*. PhD Diss., Univ. Twente, Neth.
16. Wen CY, Yu YH. 1966. A generalized method for predicting the minimum fluidization velocity. *AIChE J.* 12(3):610–12
17. Wen CY, Yu YH. 1966. Mechanics of fluidization. *Chem. Eng. Prog. Symp. Ser.* 162:100–11
18. Hill RJ, Koch DL, Ladd AJC. 2001. Moderate-Reynolds-number flows in ordered and random arrays of spheres. *J. Fluid Mech.* 448:243–78
19. Beetstra R, van der Hoef MA, Kuipers JAM. 2007. Drag force of intermediate Reynolds number flow past mono- and bidisperse arrays of spheres. *AIChE J.* 53(2):489–501
20. Tenneti S, Garg R, Subramaniam S. 2011. Drag law for monodisperse gas-solid systems using particle-resolved direct numerical simulation of flow past fixed assemblies of spheres. *Int. J. Multiph. Flow* 37(9):1072–92
21. Tang Y, Peters EAJF, Kuipers JAM, Kriebitzsch SHL, van der Hoef MA. 2015. A new drag correlation from fully resolved simulations of flow past monodisperse static arrays of spheres. *AIChE J.* 61(2):688–98
22. Syamlal M, Rogers W, O'Brien TJ. 1993. *MFIX documentation theory guide*. Tech. Note, US Dep. Energy, Morgantown, WV. **https://mfix.netl.doe.gov/doc/mfix-archive/mfix_legacy_manual/Theory.pdf**
23. Ganser GH. 1993. A rational approach to drag prediction of spherical and nonspherical particles. *Powder Technol.* 77(2):143–52
24. Hölzer A, Sommerfeld M. 2009. Lattice Boltzmann simulations to determine drag, lift and torque acting on non-spherical particles. *Comput. Fluids* 38(3):572–89
25. Hölzer A, Sommerfeld M. 2008. New simple correlation formula for the drag coefficient of non-spherical particles. *Powder Technol.* 184(3):361–65
26. Bierwisch C, Kraft T, Riedel H, Moseler M. 2009. Three-dimensional discrete element models for the granular statics and dynamics of powders in cavity filling. *J. Mech. Phys. Solids* 57(1):10–31
27. Benyahia S, Galvin JE. 2010. Estimation of numerical errors related to some basic assumptions in discrete particle methods. *Ind. Eng. Chem. Res.* 49(21):10588–605
28. Kieckhefen P, Pietsch S, Höfert M, Schönherr M, Heinrich S, Jäger FK. 2018. Influence of gas in-flow modelling on CFD-DEM simulations of three-dimensional prismatic spouted beds. *Powder Technol.* 329:167–80
29. Radl S, Radeke C, Khinast JG, Sundaresan S, eds. 2011. *Parcel-based approach for the simulation of gas-particle flows*. Presented at the 8th International Conference on CFD in Oil & Gas, Metallurgical and Process Industries, Trondheim, Nor.
30. Lu L, Yoo K, Benyahia S. 2016. Coarse-grained-particle method for simulation of liquid-solids reacting flows. *Ind. Eng. Chem. Res.* 55(39):10477–91
31. Radl S, Sundaresan S. 2014. A drag model for filtered Euler-Lagrange simulations of clustered gas-particle suspensions. *Chem. Eng. Sci.* 117:416–25
32. Li J, Kwauk M. 1994. *Particle-Fluid Two-Phase Flow: The Energy-Minimization Multi-Scale Method*. Beijing: Metall. Ind. Press
33. Ozel A, Kolehmainen J, Radl S, Sundaresan S. 2016. Fluid and particle coarsening of drag force for discrete-parcel approach. *Chem. Eng. Sci.* 155:258–67
34. Khan MJH, Hussain MA, Mansourpour Z, Mostoufi N, Ghasem NM, Abdullah EC. 2014. CFD simulation of fluidized bed reactors for polyolefin production—a review. *J. Ind. Eng. Chem.* 20(6):3919–46
35. El-Sayed SA, Noseir EH. 2019. Simulation of combustion of sesame and broad bean stalks in the free-board zone inside a pilot-scale bubbling fluidized bed combustor using CFD modeling. *Appl. Therm. Eng.* 158:113767
36. Ostermeier P, Fischer F, Fendt S, DeYoung S, Spliethoff H. 2019. Coarse-grained CFD-DEM simulation of biomass gasification in a fluidized bed reactor. *Fuel* 255:115790
37. Zhong W, Yu A, Zhou G, Xie J, Zhang H. 2016. CFD simulation of dense particulate reaction system: approaches, recent advances and applications. *Chem. Eng. Sci.* 140:16–43

38. Sun X, Sakai M. 2015. Three-dimensional simulation of gas-solid-liquid flows using the DEM-VOF method. *Chem. Eng. Sci.* 134:531–48
39. Li H, Li Y, Gao F, Zhao Z, Xu L. 2012. CFD-DEM simulation of material motion in air-and-screen cleaning device. *Comput. Electron. Agric.* 88:111–19
40. Yuan J, Wu C, Li H, Qi X, Xiao X, Shi X. 2018. Movement rules and screening characteristics of rice-threshed mixture separation through a cylinder sieve. *Comput. Electron. Agric.* 154:320–29
41. Wang S, Li H, Wang R, Wang X, Tian R, Sun Q. 2019. Effect of the inlet angle on the performance of a cyclone separator using CFD-DEM. *Adv. Powder Technol.* 30(2):227–39
42. Chu K, Chen J, Yu A. 2016. Applicability of a coarse-grained CFD-DEM model on dense medium cyclone. *Miner. Eng.* 90:43–54
43. Ji L, Chu K, Kuang S, Chen J, Yu A. 2018. Modeling the multiphase flow in hydrocyclones using the coarse-grained volume of fluid—discrete element method and mixture-discrete element method approaches. *Ind. Eng. Chem. Res.* 57(29):9641–55
44. Fitzpatrick RS, Glass HJ, Pascoe RD. 2015. CFD-DEM modelling of particle ejection by a sensor-based automated sorter. *Miner. Eng.* 79:176–84
45. Pieper C, Pfaff F, Maier G, Kruggel-Emden H, Wirtz S, et al. 2018. Numerical modelling of an optical belt sorter using a DEM-CFD approach coupled with particle tracking and comparison with experiments. *Powder Technol.* 340:181–93
46. Chen A, Wang Z, Yang J. 2016. Influence of bubble size on the fluid dynamic behavior of a DAF tank: a 3D numerical investigation. *Colloids Surf. A Physicochem. Eng. Aspects* 495:200–7
47. Liu TY, Schwarz MP. 2009. CFD-based multiscale modelling of bubble-particle collision efficiency in a turbulent flotation cell. *Chem. Eng. Sci.* 64(24):5287–301
48. Liu TY, Schwarz MP. 2009. CFD-based modelling of bubble-particle collision efficiency with mobile bubble surface in a turbulent environment. *Int. J. Miner. Proc.* 90(1–4):45–55
49. Viduka S, Feng Y, Hapgood K, Schwarz P. 2013. CFD-DEM investigation of particle separations using a sinusoidal jigging profile. *Adv. Powder Technol.* 24(2):473–81
50. Fernández XR, Nirschl H. 2013. Simulation of particles and sediment behaviour in centrifugal field by coupling CFD and DEM. *Chem. Eng. Sci.* 94:7–19
51. Ma L, Wei L, Pei X, Zhu X, Xu D. 2019. CFD-DEM simulations of particle separation characteristic in centrifugal compounding force field. *Powder Technol.* 343:11–18
52. Fatahi MR, Farzanegan A. 2018. An analysis of multiphase flow and solids separation inside Knelson Concentrator based on four-way coupling of CFD and DEM simulation methods. *Miner. Eng.* 126:130–44
53. El-Emam MA, Shi W, Zhou L. 2019. CFD-DEM simulation and optimization of gas-cyclone performance with realistic macroscopic particulate matter. *Adv. Powder Technol.* 30:2686–702
54. Wang G, Ge L, Mitra S, Evans GM, Joshi JB, Chen S. 2018. A review of CFD modelling studies on the flotation process. *Miner. Eng.* 127:153–77
55. Petit HA, Irassar EF, Barbosa MR. 2018. Evaluation of the performance of the cross-flow air classifier in manufactured sand processing via CFD-DEM simulations. *Comp. Part. Mech.* 5(1):87–102
56. Wurster DE. 1949. *Method of applying coatings to edible tablets or the like*. US Patent No. 2648609A
57. Xu BH, Yu AB. 1997. Numerical simulation of the gas-solid flow in a fluidized bed by combining discrete particle method with computational fluid dynamics. *Chem. Eng. Sci.* 52(16):2785–809
58. Hoomans BPB, Kuipers JAM, Briels WJ, van Swaaij WPM. 1996. Discrete particle simulation of bubble and slug formation in a two-dimensional gas-fluidised bed: a hard-sphere approach. *Chem. Eng. Sci.* 51(1):99–118
59. Chiesa M, Mathiesen V, Melheim JA, Halvorsen B. 2005. Numerical simulation of particulate flow by the Eulerian-Lagrangian and the Eulerian-Eulerian approach with application to a fluidized bed. *Comput. Chem. Eng.* 29(2):291–304
60. Kawaguchi T, Tanaka T, Tsuji Y. 1998. Numerical simulation of two-dimensional fluidized beds using the discrete element method (comparison between the two- and three-dimensional models). *Powder Technol.* 96(2):129–38
61. Chaikittisilp W, Taenumtrakul T, Boonsuwan P, Tanthapanichakoon W, Charinpanitkul T. 2006. Analysis of solid particle mixing in inclined fluidized beds using DEM simulation. *Chem. Eng. J.* 122(1):21–29

62. Di Renzo A, Di Maio FP. 2007. Homogeneous and bubbling fluidization regimes in DEM-CFD simulations: hydrodynamic stability of gas and liquid fluidized beds. *Chem. Eng. Sci.* 62(1):116–30
63. Tsuji T, Yabumoto K, Tanaka T. 2008. Spontaneous structures in three-dimensional bubbling gas-fluidized bed by parallel DEM-CFD coupling simulation. *Powder Technol.* 184(2):132–40
64. Norouzi HR, Mostoufi N, Mansourpour Z, Sotudeh-Gharebagh R, Chaouki J. 2011. Characterization of solids mixing patterns in bubbling fluidized beds. *Chem. Eng. Res. Des.* 89(6):817–26
65. Li T, Gopalakrishnan P, Garg R, Shahnam M. 2012. CFD-DEM study of effect of bed thickness for bubbling fluidized beds. *Particuology* 10(5):532–41
66. Luo K, Wu F, Yang S, Fan J. 2015. CFD-DEM study of mixing and dispersion behaviors of solid phase in a bubbling fluidized bed. *Powder Technol.* 274:482–93
67. Oke O, van Wachem B, Mazzei L. 2016. Lateral solid mixing in gas-fluidized beds: CFD and DEM studies. *Chem. Eng. Res. Des.* 114:148–61
68. Wang S, Luo K, Hu C, Lin J, Fan J. 2019. CFD-DEM simulation of heat transfer in fluidized beds: model verification, validation, and application. *Chem. Eng. Sci.* 197:280–95
69. Limtrakul S, Rotjanavijit W, Vatanatham T. 2007. Lagrangian modeling and simulation of effect of vibration on cohesive particle movement in a fluidized bed. *Chem. Eng. Sci.* 62(1):232–45
70. Zhenghua H, Xiang L, Huilin L, Guodong L, Yurong H, et al. 2010. Numerical simulation of particle motion in a gradient magnetically assisted fluidized bed. *Powder Technol.* 203(3):555–64
71. Pei C, Wu C-Y, England D, Byard S, Berchtold H, Adams M. 2013. Numerical analysis of contact electrification using DEM-CFD. *Powder Technol.* 248:34–43
72. Namdarkedenji R, Hashemnia K, Emdad H. 2018. Effect of flow pulsation on fluidization degree of gas-solid fluidized beds by using coupled CFD-DEM. *Adv. Powder Technol.* 29(12):3527–41
73. Kawaguchi T, Sakamoto M, Tanaka T, Tsuji Y. 2000. Quasi-three-dimensional numerical simulation of spouted beds in cylinder. *Powder Technol.* 109(1):3–12
74. Takeuchi S, Wang S, Rhodes M. 2004. Discrete element simulation of a flat-bottomed spouted bed in the 3-D cylindrical coordinate system. *Chem. Eng. Sci.* 59(17):3495–504
75. Zhao X-L, Li S-Q, Liu G-Q, Yao Q, Marshall J-S. 2008. DEM simulation of the particle dynamics in two-dimensional spouted beds. *Powder Technol.* 184(2):205–13
76. Rong L-W, Zhan J-M. 2010. Improved DEM-CFD model and validation: a conical-base spouted bed simulation study. *J. Hydrodyn. B* 22(3):351–59
77. Link JM, Cuypers LA, Deen NG, Kuipers JAM. 2005. Flow regimes in a spout-fluid bed: a combined experimental and simulation study. *Chem. Eng. Sci.* 60(13):3425–42
78. Saidi M, Basirat Tabrizi H, Grace JR, Lim CJ, Ahmadi G. 2015. Hydrodynamic and mixing characteristics of gas-solid flow in a pulsed spouted bed. *Ind. Eng. Chem. Res.* 54(32):7933–41
79. Liu M, Wen Y, Liu R, Liu B, Shao Y. 2015. Investigation of fluidization behavior of high density particle in spouted bed using CFD-DEM coupling method. *Powder Technol.* 280:72–82
80. Pietsch S, Heinrich S, Karpinski K, Müller M, Schönherr M, Kleine Jäger F. 2017. CFD-DEM modeling of a three-dimensional prismatic spouted bed. *Powder Technol.* 316:245–55
81. Nakamura H, Watano S. 2006. Numerical simulation of particle fluidization behaviors in a rotating fluidized bed. In *Studies in Surface Science and Catalysis: New Developments and Application in Chemical Reaction Engineering*, ed. H-K Rhee, I-S Nam, JM Park, pp. 505–8. Amsterdam: Elsevier
82. Nakamura H, Tokuda T, Iwasaki T, Watano S. 2007. Numerical analysis of particle mixing in a rotating fluidized bed. *Chem. Eng. Sci.* 62(11):3043–56
83. Neuwirth J, Antonyuk S, Heinrich S, Jacob M. 2013. CFD-DEM study and direct measurement of the granular flow in a rotor granulator. *Chem. Eng. Sci.* 86:151–63
84. Deb S, Tafti DK. 2014. Two and three dimensional modeling of fluidized bed with multiple jets in a DEM-CFD framework. *Particuology* 16:19–28
85. Deb S, Tafti D. 2014. Investigation of flat bottomed spouted bed with multiple jets using DEM-CFD framework. *Powder Technol.* 254:387–402
86. Feng YQ, Xu BH, Zhang SJ, Yu AB, Zulli P. 2004. Discrete particle simulation of gas fluidization of particle mixtures. *AIChE J.* 50(8):1713–28
87. Tagami N, Mujumdar A, Horio M. 2009. DEM simulation of polydisperse systems of particles in a fluidized bed. *Particuology* 7(1):9–18

88. Olaofe OO, Patil AV, Deen NG, van der Hoef MA, Kuipers JAM. 2014. Simulation of particle mixing and segregation in bidisperse gas fluidized beds. *Chem. Eng. Sci.* 108:258–69
89. Hilton JE, Mason LR, Cleary PW. 2010. Dynamics of gas-solid fluidised beds with non-spherical particle geometry. *Chem. Eng. Sci.* 65(5):1584–96
90. Zhou ZY, Pinson D, Zou RP, Yu AB. 2011. Discrete particle simulation of gas fluidization of ellipsoidal particles. *Chem. Eng. Sci.* 66(23):6128–45
91. Ma H, Xu L, Zhao Y. 2017. CFD-DEM simulation of fluidization of rod-like particles in a fluidized bed. *Powder Technol.* 314:355–66
92. Kuwagi K, Horio M. 2002. A numerical study on agglomerate formation in a fluidized bed of fine cohesive particles. *Chem. Eng. Sci.* 57(22):4737–44
93. Kuwagi K, Takano K, Horio M. 2000. The effect of tangential lubrication by bridge liquid on the behavior of agglomerating fluidized beds. *Powder Technol.* 113(3):287–98
94. Fries L, Antonyuk S, Heinrich S, Palzer S. 2011. DEM-CFD modeling of a fluidized bed spray granulator. *Chem. Eng. Sci.* 66(11):2340–55
95. Fries L, Antonyuk S, Heinrich S, Dopfer D, Palzer S. 2013. Collision dynamics in fluidised bed granulators: a DEM-CFD study. *Chem. Eng. Sci.* 86:108–23
96. Li L, Remmelgas J, van Wachem BGM, von Corswant C, Johansson M, et al. 2015. Residence time distributions of different size particles in the spray zone of a Wurster fluid bed studied using DEM-CFD. *Powder Technol.* 280:124–34
97. Azmir J, Hou Q, Yu A. 2018. Discrete particle simulation of food grain drying in a fluidised bed. *Powder Technol.* 323:238–49
98. Goldschmidt MJV, Weijers GGC, Boerefijn R, Kuipers JAM. 2003. Discrete element modelling of fluidised bed spray granulation. *Powder Technol.* 138(1):39–45
99. Link JM, Godlieb W, Deen NG, Kuipers JAM. 2007. Discrete element study of granulation in a spout-fluidized bed. *Chem. Eng. Sci.* 62(1):195–207
100. van Buijtenen MS, Deen NG, Heinrich S, Antonyuk S, Kuipers JAM. 2009. A discrete element study of wet particle-particle interaction during granulation in a spout fluidized bed. *Can. J. Chem. Eng.* 87(2):308–17
101. Sutkar VS, Deen NG, Patil AV, Salikov V, Antonyuk S, et al. 2016. CFD-DEM model for coupled heat and mass transfer in a spout fluidized bed with liquid injection. *Chem. Eng. J.* 288:185–97
102. Liu D, van Wachem BGM, Mudde RF, Chen X, van Ommen JR. 2016. Characterization of fluidized nanoparticle agglomerates by using adhesive CFD-DEM simulation. *Powder Technol.* 304:198–207
103. Dosta M, Antonyuk S, Heinrich S. 2013. Multiscale simulation of agglomerate breakage in fluidized beds. *Ind. Eng. Chem. Res.* 52(33):11275–81
104. Dosta M, Antonyuk S, Heinrich S. 2012. Multiscale simulation of the fluidized bed granulation process. *Chem. Eng. Technol.* 35(8):1373–80
105. Sen M, Barrasso D, Singh R, Ramachandran R. 2014. A multi-scale hybrid CFD-DEM-PBM description of a fluid-bed granulation process. *Processes* 2(1):89–111
106. Tamrakar A, Ramachandran R. 2019. CFD-DEM-PBM coupled model development and validation of a 3D top-spray fluidized bed wet granulation process. *Comput. Chem. Eng.* 125:249–70
107. Heinrich S, Dosta M, Antonyuk S. 2015. Multiscale analysis of a coating process in a Wurster fluidized bed apparatus *Adv. Chem. Eng.* 46:83–135
108. Kunii D, Levenspiel O, eds. 1991. *Fluidization Engineering*. Boston: Butterworth-Heinemann. 2nd ed.
109. Kaneko Y, Shiojima T, Horio M. 1999. DEM simulation of fluidized beds for gas-phase olefin polymerization. *Chem. Eng. Sci.* 54(24):5809–21
110. Kuwagi K, Mikami T, Horio M. 2000. Numerical simulation of metallic solid bridging particles in a fluidized bed at high temperature. *Powder Technol.* 109(1):27–40
111. Zhou H, Abanades S, Flamant G, Gauthier D, Lu J. 2002. Simulation of heavy metal vaporization dynamics in a fluidized bed. *Chem. Eng. Sci.* 57(14):2603–14
112. Limtrakul S, Boonsrirat A, Vatanatham T. 2004. DEM modeling and simulation of a catalytic gas-solid fluidized bed reactor: a spouted bed as a case study. *Chem. Eng. Sci.* 59(22):5225–31

113. Czok G, Ye M, van der Hoef MA, Kuipers JAM, Werther J. 2005. Modeling and chemical vapor deposition in a fluidized bed reactor based on discrete particle simulation. *Int. J. Chem. React. Eng.* 3(1). **https://doi.org/10.2202/1542-6580.1234**
114. Di Maio FP, Di Renzo A, Trevisan D. 2009. Comparison of heat transfer models in DEM-CFD simulations of fluidized beds with an immersed probe. *Powder Technol.* 193(3):257–65
115. Zhou ZY, Yu AB, Zulli P. 2010. A new computational method for studying heat transfer in fluid bed reactors. *Powder Technol.* 197(1):102–10
116. Patil AV, Peters EAJF, Kuipers JAM. 2015. Comparison of CFD-DEM heat transfer simulations with infrared/visual measurements. *Chem. Eng. J.* 277:388–401
117. Wu C, Cheng Y, Ding Y, Jin Y. 2010. CFD-DEM simulation of gas-solid reacting flows in fluid catalytic cracking (FCC) process. *Chem. Eng. Sci.* 65(1):542–49
118. Zhuang Y-Q, Chen X-M, Luo Z-H, Xiao J. 2014. CFD-DEM modeling of gas-solid flow and catalytic MTO reaction in a fluidized bed reactor. *Comput. Chem. Eng.* 60:1–16
119. Ku X, Li T, Løvås T. 2015. CFD-DEM simulation of biomass gasification with steam in a fluidized bed reactor. *Chem. Eng. Sci.* 122:270–83
120. Li J, Agarwal RK, Zhou L, Yang B. 2019. Investigation of a bubbling fluidized bed methanation reactor by using CFD-DEM and approximate image processing method. *Chem. Eng. Sci.* 207:1107–20
121. Bellan S, Kodama T, Matsubara K, Gokon N, Cho HS, Inoue K. 2019. Thermal performance of a 30 kW fluidized bed reactor for solar gasification: a CFD-DEM study. *Chem. Eng. J.* 360:1287–300
122. Jayasundara CT, Yang RY, Guo BY, Yu AB, Govender I, et al. 2011. CFD-DEM modelling of particle flow in IsaMills—comparison between simulations and PEPT measurements. *Miner. Eng.* 24(3–4):181–87
123. Lee HW, Song S, Kim HT. 2019. Improvement of pulverization efficiency for micro-sized particles grinding by uncooled high-temperature air jet mill using a computational simulation. *Chem. Eng. Sci.* 207:1140–47
124. Brosh T, Kalman H, Levy A, Peyron I, Ricard F. 2014. DEM-CFD simulation of particle comminution in jet-mill. *Powder Technol.* 257:104–12
125. Rodnianski V, Levy A, Kalman H. 2019. A new method for simulation of comminution process in jet mills. *Powder Technol.* 343:867–79
126. Takeuchi H, Nakamura H, Watano S. 2013. Numerical simulation of particle breakage in dry impact pulverizer. *AIChE J.* 59(10):3601–11
127. Kushimoto K, Ishihara S, Kano J. 2019. Development of ADEM-CFD model for analyzing dynamic and breakage behavior of aggregates in wet ball milling. *Adv. Powder Technol.* 30(6):1131–40
128. Teng S, Wang P, Zhang Q, Gogos C. 2011. Analysis of fluid energy mill by gas-solid two-phase flow simulation. *Powder Technol.* 208(3):684–93
129. Beinert S, Fragnière G, Schilde C, Kwade A. 2018. Multiscale simulation of fine grinding and dispersing processes: stressing probability, stressing energy and resultant breakage rate. *Adv. Powder Technol.* 29(3):573–83
130. Li S-Q, Marshall JS. 2007. Discrete element simulation of micro-particle deposition on a cylindrical fiber in an array. *J. Aerosol Sci.* 38(10):1031–46
131. Qian F, Huang N, Zhu X, Lu J. 2013. Numerical study of the gas-solid flow characteristic of fibrous media based on SEM using CFD-DEM. *Powder Technol.* 249:63–70
132. Qian F, Huang N, Lu J, Han Y. 2014. CFD-DEM simulation of the filtration performance for fibrous media based on the mimic structure. *Comput. Chem. Eng.* 71:478–88
133. Dong M, Li J, Shang Y, Li S. 2019. Numerical investigation on deposition process of submicron particles in collision with a single cylindrical fiber. *J. Aerosol Sci.* 129:1–15
134. Naukkarinen T, Nikku M, Turunen-Saaresti T. 2019. CFD-DEM simulations of hydrodynamics of combined ion exchange-membrane filtration. *Chem. Eng. Sci.* 208:115151
135. Li B, Dobosz KM, Zhang H, Schiffman JD, Saranteas K, Henson MA. 2019. Predicting the performance of pressure filtration processes by coupling computational fluid dynamics and discrete element methods. *Chem. Eng. Sci.* 208:115162
136. Korossis S, Bolland F, Kearney JN, Fisher J, Ingham E. 2005. Bioreactors in tissue engineering. *Top. Tissue Eng.* 2:1–23

137. Morchain J. 2017. Tools for bioreactor modeling and simulation. In *Bioreactor Modeling: Interaction between Intracellular Reactivity and Extracellular Environment in Bioreactors*, ed. J Morchain, pp. 1–27. London: ISTE
138. Yamamoto T, Yano M, Okano Y, Kino-oka M. 2018. Numerical investigation for the movement of cell colonies in bioreactors: stirring and orbital shaking tanks. *J. Chem. Eng. Jpn.* 51(5):423–30
139. Tan L, Roghair I, van Sint Annaland M. 2016. Discrete particle simulations of micro membrane-assisted fluidized beds with H2 extraction. *Int. J. Hydrogen Energy* 41(20):8719–31
140. de Jong JF, Dang TYN, van Sint Annaland M, Kuipers JAM. 2012. Comparison of a discrete particle model and a two-fluid model to experiments of a fluidized bed with flat membranes. *Powder Technol.* 230:93–105
141. Hirche D, Chew JW, Hinrichsen O. 2020. CFD-DEM study of geometry changes in an AnFMBR towards particle momentum. *Chem. Eng. J.* 379:122336
142. Norouzi HR, Zarghami R, Mostoufi N. 2017. New hybrid CPU-GPU solver for CFD-DEM simulation of fluidized beds. *Powder Technol.* 316:233–44
143. Pozzetti G, Besseron X, Rousset A, Peters B. 2018. A co-located partitions strategy for parallel CFD-DEM couplings. *Adv. Powder Technol.* 29(12):3220–32
144. Lichtenegger T, Pirker S. 2016. Recurrence CFD—a novel approach to simulate multiphase flows with strongly separated time scales. *Chem. Eng. Sci.* 153:394–410
145. Lichtenegger T. 2018. Local and global recurrences in dynamic gas-solid flows. *Int. J. Multiph. Flow* 106:125–37
146. Lichtenegger T, Peters EAJF, Kuipers JAM, Pirker S. 2017. A recurrence CFD study of heat transfer in a fluidized bed. *Chem. Eng. Sci.* 172:310–22
147. Kieckhefen P, Lichtenegger T, Pietsch S, Pirker S, Heinrich S. 2018. Simulation of spray coating in a spouted bed using recurrence CFD. *Particuology* 42:92–103
148. Lichtenegger T, Kieckhefen P, Heinrich S, Pirker S. 2019. Dynamics and long-time behavior of gas-solid flows on recurrent-transient backgrounds. *Chem. Eng. J.* 364:562–77
149. Pirker S, Lichtenegger T. 2018. Efficient time-extrapolation of single-and multiphase simulations by transport based recurrence CFD (rCFD). *Chem. Eng. Sci.* 188:65–83
150. Pirker S, Lichtenegger T. 2019. Process control of through-flow reactor operation by real-time recurrence CFD (rCFD) simulations—proof of concept. *Chem. Eng. Sci.* 198:241–52
151. He L, Tafti DK. 2019. A supervised machine learning approach for predicting variable drag forces on spherical particles in suspension. *Powder Technol.* 345:379–89
152. Yan S, He Y, Tang T, Wang T. 2019. Drag coefficient prediction for non-spherical particles in dense gas-solid two-phase flow using artificial neural network. *Powder Technol.* 354:115–24
153. Jiang Y, Kolehmainen J, Gu Y, Kevrekidis YG, Ozel A, Sundaresan S. 2019. Neural-network-based filtered drag model for gas-particle flows. *Powder Technol.* 346:403–13
154. Beck A, Flad D, Munz C-D. 2019. Deep neural networks for data-driven LES closure models. *J. Comput. Phys.* 398:108910